

# Implementation of higher-order methods for robust and efficient compositional simulation

Jiří Mikyška<sup>a,b</sup>, Abbas Firoozabadi<sup>a,\*</sup>

<sup>a</sup> Reservoir Engineering Research Institute, 385 Sherman Avenue, Suite 5, Palo Alto, CA 94306, USA

<sup>b</sup> Czech Technical University in Prague, Faculty of Nuclear Sciences and Physical Engineering, Department of Mathematics, Trojanova 13, 120 00 Prague, Czech Republic

## ARTICLE INFO

### Article history:

Received 13 February 2009

Received in revised form 10 December 2009

Accepted 21 December 2009

Available online 4 January 2010

### Keywords:

Compositional flow

Two-phase flow

Mixed finite-elements

Discontinuous Galerkin method

Monotone upwind scheme for conservation laws

Slope limiter

Gas injection

## ABSTRACT

Numerical simulation of two-phase multicomponent flow in permeable media with species transfer between the phases often requires use of higher-order methods. Unlike first-order methods, higher-order methods may be very sensitive to problem formulation. The sensitivity to problem formulation and lack of recognition have hindered the widespread use of higher-order methods in various problems including improved oil recovery and sequestration from CO<sub>2</sub> injection. In this work, we offer proper formulation of species balance equations and boundary conditions which overcome problems of formulations used previously that were detrimental to the efficiency of higher-order methods. We also present proper approximation of phase fluxes in the mixed finite element method. Our proposals remove major deficiencies in using higher-order methods in two-phase multicomponent flow. Numerical examples are presented to demonstrate robustness and efficiency of our approach.

© 2009 Published by Elsevier Inc.

## 1. Introduction

Injection of gases such as CO<sub>2</sub> in the subsurface has broad applications in oil recovery and in sequestration. In such injection schemes in addition to transfer of species between the phases, there can be substantial changes in density and viscosity of the phases from solubility and vaporization of species. For CO<sub>2</sub>, there is often an increase in liquid phase density from solubility. There is also decrease in liquid viscosity. CO<sub>2</sub> solubility may also result in swelling of the liquid phase. Depending on the transfer of species between the phases, there may be also the opposite effects. Despite much progress in the last thirty years in numerical simulation of gas injection schemes in the subsurface, efficient numerical simulation of compositional effects remains a challenging task.

There are two types of numerical schemes used for compositional simulation. In one scheme, first-order finite-difference and finite-volume methods are used. The latter is fit for unstructured grids while the former is for structured grids. One serious issue with the first-order schemes is severe numerical dispersion. Another limitation is the accuracy of flow field calculations. First-order finite-volume methods [1] have been used for two-phase flow in permeable media. Despite powerful features, these methods have inherent limitations when applied to fractured media [2].

Higher-order methods have been used in compositional models. The two main advantageous features of these methods are: (1) low numerical dispersion, and (2) accurate flow field calculations. Finite element method is the main approach in

\* Corresponding author. Tel.: +1 650 326 9172; fax: +1 650 326 9277.

E-mail addresses: [jiri.mikyska@jfifi.cvut.cz](mailto:jiri.mikyska@jfifi.cvut.cz) (J. Mikyška), [abbas.firoozabadi@yale.edu](mailto:abbas.firoozabadi@yale.edu) (A. Firoozabadi).

higher-order method for complex compositional modeling. Unlike the first-order methods, higher-order methods, especially the finite element methods, are very sensitive to proper problem formulation and proper physics. This aspect is often ignored in the literature.

In two recent papers [3,4], Hoteit and Firoozabadi have advanced the use of the combined discontinuous Galerkin (DG) and mixed-hybrid finite element (MHFE) methods for compositional modeling. The combined algorithm provides a powerful tool for multicomponent flow modeling of two phases in complex permeable media. In an earlier work [5], Chen et al. have applied the combined method for the electric field and convection. In the problem of interest to us, the DG has low numerical dispersion and the MHFE gives accurate calculation of the flow field. In further testing of the combined approach we have found that in some cases the code crashes. We have also seen some oscillations in contour plot of the species concentration. A close examination has shown that there may exist some fundamental issues with formulation in the literature and in our own work [3,4]. These issues may not affect first-order finite-difference and finite-volumes methods, but can affect higher-order methods. Proper formulation of the problem has not been discussed in the literature to the best of our knowledge. These issues are common to any higher-order method. In this work, we will use a combination of mixed-hybrid finite element method for the pressure equation and either discontinuous Galerkin finite element method or higher-order finite-volume (FV) scheme of the MUSCL (monotone upwind-centered scheme for conservation laws) type for the transport equations.

In this paper, for the sake of completeness, we present the formulation of two-phase flow with species transfer between the phases in permeable media. We first provide the flow equations, and then present boundary conditions. Boundary conditions in two-phase compositional flow are subtle issues. Next we derive the numerical schemes and then introduce the numerical algorithm for computations. Upwinding of different coefficients in the equations is discussed in detail. This issue also deserves much attention. At the end, we provide six numerical examples to demonstrate the performance of both algorithms. The results reveal that proper implementation of physical concepts allows efficient calculation and robustness of the algorithm. The work is ended with summary and conclusions.

## 2. Model equations

Consider two-phase (oil and gas) flow with  $n_c$ -components in permeable media without capillarity and diffusion at a constant temperature  $T$ . The transport of the components is described by the following molar balance equations

$$\phi \frac{\partial c z_i}{\partial t} + \nabla \cdot (c_o x_{oi} \mathbf{v}_o + c_g x_{gi} \mathbf{v}_g) = F_i, \quad i = 1, \dots, n_c, \tag{1}$$

where  $\phi$  is the porosity,  $c$  is the overall molar density,  $z_i$  is the mole fraction of  $i$ th component,  $c_o$ ,  $c_g$ ,  $x_{oi}$  and  $x_{gi}$  are the oil and gas molar densities and oil and gas molar fractions, respectively, and  $F_i$  describes distribution of the sources/sinks of the  $i$ th component. Other symbols will be defined shortly.

The above system is written in the following form for numerical implementation [3–6]

$$\phi \frac{\partial c z_i}{\partial t} + \nabla \cdot (c_o x_{oi} \mathbf{v}_o + c_g x_{gi} \mathbf{v}_g) = F_i, \quad i = 1, \dots, n_c - 1, \tag{2a}$$

$$\phi \frac{\partial c}{\partial t} + \nabla \cdot (c_o \mathbf{v}_o + c_g \mathbf{v}_g) = F \equiv \sum_{i=1}^n F_i. \tag{2b}$$

The species balance equations in the form presented in (2a) and (2b) is fit for implementation in the first-order finite-difference and first-order finite-volume schemes. This is the form that all the works in the literature is based on. However, after much examination we suspected that (2a) and (2b) give oscillation in species profile in the implementation of the higher-order method used in our work. The problem was definitively solved when the species balance equations in the form given by (1) was implemented. We also observed larger time steps in our implementation. Later in this work we will discuss the reasoning behind use of (1).

The oil and gas phase velocities  $\mathbf{v}_o$  and  $\mathbf{v}_g$  are described by Darcy’s laws,

$$\mathbf{v}_\alpha = -\lambda_\alpha(S_\alpha) \mathbf{K} (\nabla p - \rho_\alpha \mathbf{g}), \quad \alpha \in \{o, g\}, \tag{3}$$

where  $\lambda_\alpha$  is the  $\alpha$ -phase mobility,  $\mathbf{K}$  is the permeable medium intrinsic permeability,  $p$  is the pressure,  $\rho_\alpha$  is the  $\alpha$ -phase density, and  $\mathbf{g}$  is the gravity acceleration vector. In (1), (2a) and (2b),  $t$  denotes the time. The viscosities hidden in the mobility terms are estimated based on the methodology of Lohrenz et al. [7].

Using the concept of volume-balance, one can derive the following pressure equation (see [6]),

$$\phi c_f \frac{\partial p}{\partial t} + \sum_{i=1}^{n_c} \bar{v}_i \nabla \cdot (c_o x_{oi} \mathbf{v}_o + c_g x_{gi} \mathbf{v}_g) = \sum_{i=1}^{n_c} \bar{v}_i F_i, \tag{4}$$

where  $c_f$  is the total fluid compressibility and  $\bar{v}_i$  is the total partial molar volume of the  $i$ th component (see [8] for details).

The splitting of components between the phases is given by the following thermodynamic equilibrium equations

$$f_{oi}(x_{o1}, \dots, x_{on_c-1}, p; T) = f_{gi}(x_{g1}, \dots, x_{gn_c-1}, p; T), \quad i = 1, \dots, n_c, \quad (5a)$$

$$z_i = (1 - \nu)x_{oi} + \nu x_{gi}, \quad i = 1, \dots, n_c, \quad (5b)$$

$$\sum_{i=1}^{n_c} x_{oi} = \sum_{i=1}^{n_c} x_{gi} = \sum_{i=1}^{n_c} z_i = 1, \quad (5c)$$

where  $f_{oi}$  and  $f_{gi}$  represent fugacities of the  $i$ th component in the respective phase, and  $\nu$  is the gas mole fraction.

The phase and volumetric behavior is modeled using the Peng–Robinson equation of state (PR-EOS) [9] in the form

$$\rho_\alpha = c_\alpha \sum_{i=1}^{n_c} x_{\alpha i} M_i, \quad c_\alpha = \frac{p}{Z_\alpha R T}, \quad (6)$$

$$Z_\alpha^3 - (1 - B_\alpha) Z_\alpha^2 + (A_\alpha - 3B_\alpha^2 - 2B_\alpha) Z_\alpha - (A_\alpha B_\alpha - B_\alpha^2 - B_\alpha^3) = 0,$$

where  $M_i$  is the molar weight of the  $i$ th component,  $R$  is the universal gas constant, and  $A_\alpha$  and  $B_\alpha$  are the parameters of the PR-EOS which depend on pressure, temperature and respective phase composition (see [8]).

For evaluation of the phase mobilities in (3), the phase saturations are calculated from

$$S_o = \frac{c}{c_o} (1 - \nu), \quad S_g = \frac{c}{c_g} \nu. \quad (7)$$

The saturation constraint  $S_o + S_g = 1$  then provides an additional condition

$$1 - c \left( \frac{1 - \nu}{c_o} + \frac{\nu}{c_g} \right) = 0, \quad (8)$$

from which we can evaluate  $c$  independent of the transport equation (1). Obviously, the system is over determined; we have one more equation than the unknowns. In the computations, the value of  $c$  is determined from Eq. (1) and the constraint equation (8) is used as a criterion for the selection of a time step.

The above equations pertain to the condition when both phases are present. When the system is only in a single-phase, then the equation system must be modified. When only  $\alpha$ -phase is present, the fugacity equality (5a) has no relevance and the rest of the equations are transformed into a simpler system by identifying  $c_\alpha$  with  $c$ ,  $z_i$  with  $x_{\alpha i}$ , setting  $S_\alpha$  to one and  $\nu$  to either one or zero depending on the phase identity.

### 3. Initial and boundary conditions

In this work we found that the implementation of boundary conditions at the horizontal impermeable walls in two-phase was critical for successful computations. We also found that the current implementation based on literature formulation gives inconsistent pressure in the grid cells at the horizontal impermeable walls.

To define a well-posed problem, the system of equations formulated in the previous section must be completed by appropriate initial and boundary conditions. The pressure equation (4) is parabolic with respect to pressure. Therefore, we have to provide an initial condition for pressure at each point of the domain  $\Omega$ . As we will use the total molar flux formulation (introduced later), we have to provide either pressure (Dirichlet boundary condition) or normal component of total molar flux (Neumann boundary condition) at each boundary point  $\mathbf{x} \in \partial\Omega$ . The transport equation (1) are hyperbolic type and of the first-order with respect to  $cz_i$ . It is, therefore, necessary to prescribe initial molar density and mole fractions of all components in the mixture at all points inside the domain  $\Omega$ . The boundary values of molar density and composition can be prescribed at the inflow boundary. On the other hand, the values at the outflow boundary will be computed.

The injection/production wells can be represented by the source/sink terms, respectively. The whole boundary can then be represented by impermeable walls. The condition for impermeable walls is specified in the literature by

$$\mathbf{v}_\alpha \cdot \mathbf{n} = -\lambda_\alpha (S_\alpha) \mathbf{K} (\nabla p - \rho_\alpha \mathbf{g}) \cdot \mathbf{n} = 0, \quad \alpha \in \{o, g\}, \quad (9)$$

where  $\mathbf{n}$  is the outer normal vector. Use of the above equation in two-phase region (where  $\lambda_\alpha \neq 0$  for both  $\alpha \in \{o, g\}$ ) gives

$$\nabla p \cdot \mathbf{n} = \rho_o \mathbf{g} \cdot \mathbf{n} \quad \text{and} \quad \nabla p \cdot \mathbf{n} = \rho_g \mathbf{g} \cdot \mathbf{n}. \quad (10)$$

Note that there are two distinct pressure gradients at the wall when the phase densities are not the same. While there is no issue for a vertical impermeable wall due to absence of gravity term, there is a problem when (9) is used at the horizontal boundaries. An appropriate boundary condition in two-phase state is the use of

$$(c_o \mathbf{v}_o + c_g \mathbf{v}_g) \cdot \mathbf{n} = 0, \quad (11)$$

which prescribes the normal component of the total molar flux to be zero. The boundary condition (11) can be readily enforced using the MHFE formulation to be presented in the following section. Condition given by (11) implies that if one phase is flowing out of the domain  $\Omega$ , the other phase is flowing in at the same point. According to the above discussion, the composition of the inflow phase can be prescribed, while the composition of the outflow phase is computed. The molar balance for each component at the wall is prescribed as

$$c_o X_{oi} \mathbf{v}_o \cdot \mathbf{n} + c_g X_{gi} \mathbf{v}_g \cdot \mathbf{n} = 0. \tag{12}$$

The condition given by (12) states that the total molar flux of each individual component at the boundary is zero. The composition of the inflow phase is computed from the composition of the outflow phase so that (12) holds.

#### 4. Numerical solution

The system of Eqs. (1)–(5c) is discretized using the implicit pressure explicit composition (IMPEC) scheme. The pressure equation is solved using the mixed-hybrid finite element (MHFE) method of the lowest order providing accurate approximations of phase fluxes that are consequently used in transport modeling. The transport equations are treated either by the discontinuous Galerkin (DG) method or a higher-order finite-volume scheme such as the monotonic upwind-centered scheme for conservation laws (MUSCL, see [10–14]). Higher-order methods generally require data reconstruction using a slope limiter that must be carried out to avoid spurious oscillations. In this section we will give details of the methods for a 2D rectangular grid.

##### 4.1. Discretization of the total molar flux

We use the concept of total molar flux rather than total velocity that was used in [4]. This is due to the fact that total volumetric velocity is not preserved when composition is not the same on the two sides of the interface. Because the mobility  $\lambda_\alpha$  can be zero at extreme saturations, the total molar flux  $\mathbf{q}$  is introduced

$$\mathbf{q} = c_o \mathbf{v}_o + c_g \mathbf{v}_g = - \sum_{\alpha'} c_{\alpha'} \lambda_{\alpha'} \mathbf{K} (\nabla p - \rho \mathbf{g}), \tag{13}$$

where  $\rho = f_o \rho_o + f_g \rho_g$ , and  $f_\alpha = c_\alpha \lambda_\alpha / \sum_{\alpha'} c_{\alpha'} \lambda_{\alpha'}$ . Note that unlike coefficients  $c_\alpha \lambda_\alpha$  in the phase fluxes, the coefficient  $\sum_{\alpha'} c_{\alpha'} \lambda_{\alpha'}$  in (13) is always positive as at least one of the phases is mobile. We then solve (13) in terms of the pressure gradient

$$\nabla p = - \frac{1}{\sum_{\alpha'} c_{\alpha'} \lambda_{\alpha'}} \mathbf{K}^{-1} \mathbf{q} + \rho \mathbf{g}. \tag{14}$$

Eq. (14) can be substituted in Darcy’s laws given by (3) to obtain the following expression for phase molar fluxes

$$\mathbf{q}_\alpha \equiv c_\alpha \mathbf{v}_\alpha = f_\alpha (\mathbf{q} - \mathbf{G}_\alpha), \tag{15}$$

where

$$\mathbf{G}_\alpha = \begin{cases} c_o \lambda_o (\rho_o - \rho_g) \mathbf{K} \mathbf{g} & \alpha = g, \\ c_g \lambda_g (\rho_g - \rho_o) \mathbf{K} \mathbf{g} & \alpha = o. \end{cases} \tag{16}$$

The total molar flux is approximated using the lowest order Raviart–Thomas elements as

$$\mathbf{q}_K = \sum_{E \in \partial K} q_{K,E} \mathbf{w}_{K,E}, \tag{17}$$

where  $q_{K,E}$  is the normal component of the total molar flux over the edge  $E$  of element  $K$  with respect to outer normal, and  $\mathbf{w}_{K,E}$  denotes the  $RT_0$  basis functions (see Appendix A). The total flux can be expressed as a function of cell-average pressure  $p_K$ , traces of pressure on element faces  $tp_{K,E}$  as follows

$$q_{K,E} = a_{K,E} p_K - \sum_{E' \in \partial K} b_{K,E,E'} tp_{K,E'} + d_{K,E}, \tag{18}$$

where  $a_{K,E}$ ,  $b_{K,E,E'}$ , and  $d_{K,E}$  are coefficients which depend on the mesh geometry and on the local values of total mobility. Evaluation of these coefficients is detailed in Appendix A. The total flux continuity leads to the following equation on edge  $E = K \cap K'$  between neighboring elements  $K$  and  $K'$

$$q_{K,E} + q_{K',E} = 0, \quad K \cap K' = E. \tag{19}$$

Using (18), we derive

$$a_{K,E} p_K - \sum_{E' \in \partial K} b_{K,E,E'} tp_{K,E'} + d_{K,E} + a_{K',E} p_{K'} - \sum_{E' \in \partial K'} b_{K',E,E'} tp_{K',E'} + d_{K',E} = 0, \tag{20}$$

In this work, we use Eq. (11) to obtain the following condition for boundary edges  $E \subset \partial \Omega$  adjacent to an element  $K$

$$q_{K,E} = 0, \tag{21}$$

whence

$$a_{K,E} p_K - \sum_{E' \in \partial K} b_{K,E,E'} tp_{K,E'} + d_{K,E} = 0. \tag{22}$$

The system of Eqs. (20) and (22) can be rewritten in the matrix form as

$$\mathbf{R}^T \mathbf{P} - \mathbf{M} \mathbf{T} \mathbf{P} = \mathbf{V}, \quad (23)$$

where

$$\mathbf{R} \in \mathbb{R}^{N_K \cdot N_E}, \quad \mathbf{R}_{K,E} = \mathbf{a}_{K,E}, \quad (24a)$$

$$\mathbf{M} \in \mathbb{R}^{N_E \cdot N_E}, \quad \mathbf{M}_{E,E'} = \sum_{K:E,E' \in \partial K} \mathbf{b}_{K,E,E'}, \quad (24b)$$

$$\mathbf{V} \in \mathbb{R}^{N_E}, \quad \mathbf{V}_E = \sum_{K:E \in \partial K} \mathbf{d}_{K,E}, \quad (24c)$$

$N_K$  denotes the number of element cells,  $N_E$  number of mesh edges,  $\mathbf{P} \in \mathbb{R}^{N_K}$  is the vector of cell-average pressures (indexed by elements), and  $\mathbf{T} \mathbf{P} \in \mathbb{R}^{N_E}$  is the vector of pressure traces indexed by mesh edges.

#### 4.2. Approximation of the pressure equation

We use (15) to rewrite the pressure equation given by (4) in terms of the total molar flux as

$$\phi c_f \frac{\partial p}{\partial t} + \sum_{i=1}^{n_c} \bar{v}_i \nabla \cdot (m_i \mathbf{q} - \mathbf{s}_i) = \sum_{i=1}^{n_c} \bar{v}_i F_i, \quad (25)$$

where  $m_i = x_{oi} f_o + x_{gi} f_g$ , and  $\mathbf{s}_i = x_{oi} f_o \mathbf{G}_o + x_{gi} f_g \mathbf{G}_g$ . This equation is integrated over each element  $K$  of the mesh. Assuming that the total compressibility and the total partial molar volumes are element-wise constant, we use the divergence theorem to rewrite the last equation in the following form

$$\phi_K c_{f,K} |K| \frac{\partial p_K}{\partial t} + \sum_{i=1}^{n_c} \bar{v}_{i,K} \sum_{E \in \partial K} \int_E (m_{i,K,E} \mathbf{q}_{K,E} - \mathbf{s}_{i,K,E} \cdot \mathbf{n}_{K,E}) = \sum_{i=1}^{n_c} \bar{v}_{i,K} F_{i,K} |K|, \quad (26)$$

where  $|K|$  is the area of element  $K$ . The flux in this equation can be eliminated using (18). The backward Euler scheme for discretization of the time derivative is employed, in which all coefficients are evaluated explicitly using the values from previous time level. We end up with the following system

$$\mathbf{D} \mathbf{P}^{n+1} - \tilde{\mathbf{R}} \mathbf{T} \mathbf{P}^{n+1} = \mathbf{G}, \quad (27)$$

where the index  $n+1$  denotes the time level,  $\mathbf{D} \in \mathbb{R}^{N_K \cdot N_K}$  is a diagonal matrix with diagonal components

$$D_K = \frac{\phi_K c_{f,K} |K|}{\Delta t} + \sum_{i=1}^{n_c} \bar{v}_{i,K} \sum_{E \in \partial K} \int_E m_{i,K,E} a_{K,E},$$

$\tilde{\mathbf{R}} \in \mathbb{R}^{N_K \cdot N_E}$  is a rectangular matrix with components

$$\tilde{\mathbf{R}}_{K,E'} = \sum_{i=1}^{n_c} \bar{v}_{i,K} \sum_{E \in \partial K} \int_E m_{i,K,E} b_{K,E,E'},$$

and  $\mathbf{G} \in \mathbb{R}^{N_K}$  is a right side vector with components

$$G_K = \frac{\phi_K c_{f,K} |K|}{\Delta t} p_K^n - \sum_{i=1}^{n_c} \bar{v}_{i,K} \sum_{E \in \partial K} \int_E (m_{i,K,E} d_{K,E} - \mathbf{s}_{i,K,E} \cdot \mathbf{n}_{K,E}) + |K| \sum_{i=1}^{n_c} \bar{v}_{i,K} F_{i,K}.$$

All the coefficients  $m_{i,K,E}$  and  $\mathbf{s}_{i,K,E}$  are evaluated using the average values inside element  $K$ , i.e. we should write  $m_{i,K}$ , and  $\mathbf{s}_{i,K}$  instead of  $m_{i,K,E}$  and  $\mathbf{s}_{i,K,E}$ , respectively. Note that no upwinding is possible here because of implicit treatment of pressure. Moreover, the pressure equation (4) is not in the divergence form which implies that the volume-balance (which is the basis of the pressure equation) is not satisfied exactly by the numerical solution. This should not influence the balance of total molar flux explicitly enforced using (19).

#### 4.3. Approximation of the phase fluxes

One of the most important issues in this work is proper approximation of the phase fluxes  $\mathbf{q}_\alpha = f_\alpha (\mathbf{q} - \mathbf{G}_\alpha)$ . In this respect we have advanced the procedure outlined in [15]. At first the system of Eqs. (23) and (27) for pressures  $\mathbf{P}$  and traces of pressure  $\mathbf{T} \mathbf{P}$  at a new time level must be solved. Here we can take advantage of the fact that the matrix  $\mathbf{D}$  is diagonal with non-zero diagonal elements, and thus invertible. Therefore, we can combine (23) and (27) to derive the following system of equations for pressure traces

$$(\mathbf{M} - \mathbf{R}^T \mathbf{D}^{-1} \tilde{\mathbf{R}}) \mathbf{T} \mathbf{P}^{n+1} = \mathbf{R}^T \mathbf{D}^{-1} \tilde{\mathbf{R}} \mathbf{G}. \quad (28)$$

Once we solve for traces of pressure  $TP^{n+1}$ , the cell-average pressure  $P$  can be updated using (27). Then we can evaluate the total molar flux from (18). Eq. (19) guarantees the balance of total molar flux over the element edges. However, when evaluating the phase fluxes using (15), the local values of  $f_\alpha$  and  $\mathbf{G}_\alpha$  cannot be used as this would lead to non-matching phase fluxes at element edges. To obtain phase fluxes that are balanced at the mesh edges, the values of  $\rho_\alpha$  used in  $\mathbf{G}_\alpha$  in (15) are taken as an arithmetic average of the neighboring cell values, while  $c_{\alpha'}\lambda_{\alpha'}$  and  $c_{\alpha'}\lambda_{\alpha'}$  in  $f_\alpha$  are taken from the upwind side with respect to  $\mathbf{v}_\alpha$ . In computing phase fluxes (note that  $\mathbf{q}_\alpha$  is not available yet), we denote by  $\alpha$  the phase for which

$$\text{sgn} \mathbf{q}_{K,E} \cdot \mathbf{n}_{K,E} = -\text{sgn} \mathbf{G}_\alpha \cdot \mathbf{n}_{K,E},$$

where  $c_{\alpha'}\lambda_{\alpha'}$  and  $c_{\alpha'}\lambda_{\alpha'}$  are evaluated arbitrarily, e.g. by setting  $c_{\alpha'}\lambda_{\alpha'} = c_{\alpha'}\lambda_{\alpha'} = 1$ ; the primed phase  $\alpha'$  denotes the other phase. The use of the above expression is always possible because the total flux has been evaluated and  $\mathbf{G}_\alpha$  and  $\mathbf{G}_{\alpha'}$  (with  $c_{\alpha'}\lambda_{\alpha'}$  and  $c_{\alpha'}\lambda_{\alpha'}$  set to 1) are pointing in the opposite directions. Now we can predict the sign of  $q_{\alpha',K,E}$ , which has the same sign as of  $q_{K,E}$ , independent of the actual value of  $c_{\alpha'}\lambda_{\alpha'}$ , which is always non-negative, in (15). Using the known sign of  $q_{\alpha',K,E}$ , we can choose the upwind value of  $c_{\alpha'}\lambda_{\alpha'}$  used in the computation of  $\mathbf{G}_\alpha$ . We can now evaluate  $q_{\alpha',K,E}$  and finally the actual value of  $\lambda_{\alpha'}$  is estimated and then the actual value of  $q_{\alpha',K,E}$  can be determined. Note that this procedure is not consistent with the way we treated flux in the discretization of pressure equation, but it ensures the balance of phase velocities, which is important for correct treatment of mass balance in the transport. Our suggested procedure for calculation of individual interface phase velocities allows robust calculations and alleviates a deficiency in previous work [4].

#### 4.4. Approximation of components transport

We discuss two methods for approximation of the components transport equations: (1) the discontinuous Galerkin finite element method, and (2) the MUSCL-type finite-volume scheme.

##### 4.4.1. Discontinuous Galerkin finite element method

The components transport equation (1) are discretized using the discontinuous Galerkin finite element method. On each rectangular element  $K$ , the unknown concentration is approximated using a linear function. Note that in a rectangular element, there is no need for 4 degrees of freedom because the interpolant is allowed to be discontinuous in DG method. Assuming such an approximation in the form

$$cz_{i,K} = \sum_{l=1}^3 cz_{i,K}^l \varphi_{K,l}, \quad c_\alpha x_{\alpha i,K} = \sum_{l=1}^3 c_\alpha x_{\alpha i,K}^l \varphi_{K,l}, \tag{29}$$

where functions  $\varphi_{K,l}$  form a basis of a local approximation space (detailed in Appendix B), we multiply (1) by a test function, integrate over the element  $K$  and integrate by parts to obtain

$$\int_K \phi \frac{\partial cz_{i,K}}{\partial t} \varphi_{K,j} - \int_K (x_{oi,K} \mathbf{q}_o + x_{gi,K} \mathbf{q}_g) \cdot \nabla \varphi_{K,j} + \sum_{E \in \partial K} \int_E (x_{\alpha i,K,E} \mathbf{q}_\alpha + x_{\beta i,K,E} \mathbf{q}_\beta) \cdot \mathbf{n}_{K,E} \varphi_{K,j} = \int_K F_i \varphi_{K,j} \tag{30}$$

for each  $j \in \{1, 2, 3\}$ . In the surface integral, the  $x_{\alpha i,K,E}$  ( $\alpha \in \{o, g\}$ ) denotes the value of concentration upwind with respect to  $\mathbf{q}_\alpha$  defined as

$$x_{\alpha i,K,E} = \begin{cases} x_{\alpha i,K,E} & \text{if } q_{\alpha,K,E} \equiv \mathbf{q}_\alpha \cdot \mathbf{n}_{K,E}|E| \geq 0, \\ x_{\beta i,K',E} & \text{if } q_{\alpha,K,E} \equiv \mathbf{q}_\alpha \cdot \mathbf{n}_{K,E}|E| < 0, \end{cases} \tag{31}$$

where we assume that  $E = K \cap K'$  is a common edge between the neighboring elements  $K$  and  $K'$ . If  $E$  is a boundary edge, then the Dirichlet boundary conditions on the influx part of the boundary can be applied readily at this stage. Note that the values  $x_{\alpha i,K,E}$  and  $x_{\beta i,K',E}$  in (31) result from the evaluation of the two-phase flash at the element edges using the values of temperature  $T$ , pressure trace  $TP$  and overall molar composition  $z_i$  at that edge. The value of  $z_i$  at the edge is computed from the value of  $z_i$  in the element center using the slopes provided by the DG method. On the other hand, the values  $x_{\alpha i,K}$  in the second integral on the left hand side of (29) is evaluated by the two-phase flash at temperature  $T$ , average element pressure  $P$  and overall molar composition  $z_i$  at the element center. This implies that five flashes must be performed on every element.

Substituting (29) into (30), we derive the following semi-discrete scheme

$$\phi_K \sum_{l=1}^3 \frac{dcz_{i,K}^l}{dt} M_{j,l}^K - \sum_{\alpha \in \{o,g\}} \sum_{l=1}^3 x_{\alpha i,K} \sum_{E \in \partial K} q_{\alpha,K,E} M_{j,l}^{K,E} + \sum_{E \in \partial K} \sum_{\alpha \in \{o,g\}} x_{\alpha i,K,E} q_{\alpha,K,E} M_j^E = \int_K F_i \varphi_{K,j}. \tag{32}$$

The matrices  $M^K$ ,  $M^E$ , and  $M^{K,E}$  are defined and their elements are evaluated in Appendix B. The matrix  $M^K$  is diagonal, and thus the forward Euler scheme leads to an explicit scheme in terms of  $cz_{i,K}^l$  with 3 degrees of freedom per element.

##### 4.4.2. Higher-order finite-volume method of the MUSCL-type

An alternative method for the discretization of the transport equation (1) is the higher-order finite-volume method. There are plenty of methods available (see [1]); in this paper we will discuss the monotonic upwind-centered scheme for conservation laws (MUSCL) by van Leer developed in a series of papers [10–14].

To develop the scheme, Eq. (1) are integrated over an arbitrary rectangular element  $K$ . After using the divergence theorem, we have

$$\int_K \phi \frac{\partial c_{i,K}^1}{\partial t} + \sum_{E \in \partial K} \int_E (\widetilde{x}_{oi,K,E} \mathbf{q}_o + \widetilde{x}_{gi,K,E} \mathbf{q}_g) \cdot \mathbf{n}_{K,E} = \int_K F_i, \quad (33)$$

where the  $\widetilde{x}_{\alpha i,K,E}$  ( $\alpha \in \{o, g\}$ ) denotes the value of concentration upwinded with respect to  $\mathbf{q}_\alpha$  defined by (31). Eq. (33) describes evolution of the average values of the overall molar densities  $c_{i,K}$  at every element. Unlike the DG scheme, the slopes of the solution are not described by an evolution equation as in (30), but rather reconstructed by using the average values of  $c_{zi}$  in the neighboring elements. In case of the rectangular mesh, the reconstruction carried out using central difference quotients as

$$c_{i,K}^2 = \frac{c_{i,R} - c_{i,L}}{4}, \quad c_{i,K}^3 = \frac{c_{i,T} - c_{i,B}}{4}, \quad (34)$$

where  $K$  denotes an element and  $R, L, T, B$  are its right, left, top, and right neighbor, respectively. The upper index  $l \in \{1, 2, 3\}$  in  $c_{i,K}^l$  is used to distinguish between the central value ( $l = 1$ ) and gradients of  $c_{i,K}$  in the  $x$  and  $y$  direction ( $l = 2, 3$ ) to keep the notation consistent with the one used in the derivation of the DG scheme (see also Appendix B). At boundary elements, the slope in the direction perpendicular to the boundary is set to zero for simplicity. After the slopes of  $c_{zi}$  have been reconstructed, the five flashes at every elements are performed to obtain equilibrium compositions  $x_{\alpha i,K}$  at element centers (using the average element pressure and overall composition) and  $x_{\alpha i,K,E}$  at element faces (using the traces of pressures, and overall composition evaluated at element faces evaluated in terms of the average values and reconstructed slopes). The values  $x_{\alpha i,K,E}$  are then used to evaluate  $\widetilde{x}_{\alpha i,K,E}$  needed in (33) using upwinding (31). Finally, the resulting FV-MUSCL scheme reads as

$$\phi_K \frac{dc_{i,K}^1}{dt} |K| + \sum_{E \in \partial K} \sum_{\alpha \in \{o, g\}} \widetilde{x}_{\alpha i,K,E} \mathbf{q}_{\alpha,K,E} = \int_K F_i. \quad (35)$$

#### 4.5. Slope limiter

To avoid unphysical oscillations in the numerical solution, both methods are stabilized by using an appropriate slope limiter. In case of the discontinuous element-wise linear approximation on a rectangular grid, the slope limiting can be carried out in a simple way using two 1D limiters in the directions of  $x$  and  $y$  axes. The idea of the method is to modify the solution resulting from the DG step after each time step so that the average value of each molar concentration is not modified and the slopes are adjusted so that the values of concentrations at any edge are between the minimum and maximum values of concentrations in adjacent cells. The implementation follows closely the description in Appendix B1 in [3]. As mentioned in Appendix B, our degrees of freedom at each element are: (1) the average value of molar concentration, (2) the difference between the value in the center of the element and the value on the right edge, and (3) the difference between the value in the center of the element and the value on the top edge, which allows for a straightforward implementation of the limiter. Also, the classical first-order finite-volume upwind method can be mimicked easily by setting the differences between the two edge values and the central value to zero.

As mentioned above, the formulation given by (2) is used instead of the original system given by (1) in the literature. When using the first-order finite-volume method, both formulations work equally well. However, there is a complication when (2) is employed in a higher-order method, such as DG or MUSCL, that requires the use of a slope limiter. Here, the use of the original system of Eq. (1) is more straightforward. After each step of DG method the limiter provides bounds  $c_{i,min}$  and  $c_{i,max}$  for each boundary value of  $c_{zi}$  and the slope may be manipulated so that the inequalities

$$c_{i,min} \leq c_{zi} \leq c_{i,max} \quad (36)$$

hold for each  $i = 1, \dots, n_c$ . The value of overall molar concentration is then evaluated as

$$c = \sum_{i=1}^{n_c} c_{zi}, \quad (37)$$

which fulfills

$$\sum_{i=1}^{n_c} c_{i,min} \leq c \leq \sum_{i=1}^{n_c} c_{i,max}. \quad (38)$$

If the alternative formulation based on (2) is used, then the limiter would provide bounds  $c_{i,min}$  and  $c_{i,max}$  on  $c_{zi}$  for  $i = 1, \dots, n_c - 1$  and bounds  $c_{min}$  and  $c_{max}$  on  $c$ . The slopes of these variables would be manipulated so that

$$c_{i,min} \leq c_{zi} \leq c_{i,max}, \quad i = 1, \dots, n_c - 1, \quad (39)$$

$$c_{min} \leq c \leq c_{max}.$$

From these inequalities we can derive the following bounds on  $cZ_{n_c}$

$$c_{max} - \sum_{i=1}^{n_c-1} cZ_{i,min} \leq cZ_{n_c} = c - \sum_{i=1}^{n_c-1} cZ_i \leq c_{max} - \sum_{i=1}^{n_c-1} cZ_{i,min}, \tag{40}$$

which are inconsistent with the bounds given by Eq. (36) for  $i = n_c$  and lead to creation of unphysical oscillations in the last component molar concentration. After several time steps, these oscillations spoil the other components profiles too. The problem could be solved by a special version of limiter for  $c$  that would enforce the correct bounds on  $cZ_{n_c}$ , but this would lead to an unnecessary complicated code which would be more difficult to debug. The straightforward solution is to use the original system of Eq. (1).

### 5. Computational algorithm

The computation proceeds in the following steps:

1. Read the initial temperature and distribution of pressure and overall molar concentrations of all components. There is only one value of temperature for the whole domain.
2. Perform the flash calculations to obtain number of phases and phase composition at the initial pressure, temperature, and overall composition at element centers and at element faces.
3. Use the Lohrentz et al. method to evaluate the phase viscosities.
4. Repeat the following steps until a predetermined simulation time is reached.
  - (a) Assemble and solve the system (28) for traces of pressure  $TP$ .
  - (b) Evaluate cell-average pressures  $P$  locally on each element using (27).
  - (c) Calculate fluxes using the procedure described in Section 4.3.
  - (d) Compute new overall composition using one explicit Euler time step of the DG scheme (32) or FV-MUSCL scheme (35).
  - (e) If the FV-MUSCL scheme was used, reconstruct the slopes of  $cZ_i$  at every element using (34).
  - (f) Apply the slope limiter.
  - (g) Perform the phase stability analysis and flash calculation to obtain number of phases and phase composition at the new pressure, temperature and overall composition at element centers and at element faces.
  - (h) Update phase viscosities.

### 6. Results of numerical computations

In this section, we present results of six examples that were carried out using the implementation of the method described in this paper. All the problems were solved on a 2D rectangular domain  $50 \times 50$  m with a rectangular grid using a HP xw9400 RedHat WS 4 workstation with the Dual-Core AMD Opteron 2216 CPU at 2.4 GHz and 4 GB memory. The relative permeability data for all examples are given in Table 1.

#### 6.1. Example 1

The first problem is the displacement of propane by methane in a horizontal 2D domain (i.e. no gravity). Methane is injected in the lower left corner, displacing propane that is produced in the upper right corner. The initial data of the problem

**Table 1**  
Relative permeability used in Examples 1–6.

Examples	1–4	5 and 6
Relative permeability model type	Linear	Quadratic
Residual gas saturation	0	0.0
Residual oil saturation	0	0.3

**Table 2**  
Relevant data for Examples 1 and 2.

Injection fluid (mole fraction)	1.0 $C_1$	0.0 $C_3$
Initial fluid (mole fraction)	0.0 $C_1$	1.0 $C_3$
Initial pressure at the bottom (bar)	50	
Temperature (K)	397	
Porosity (fraction)	0.2	
Permeability (md)	10	
Injection rate (m <sup>2</sup> /day) at $p = 1$ atm, $T = 293$ K	42.5	

given in Table 2 are chosen so that the mixture stays in single-phase gas state during whole simulation. We fix the injection rate (given in Table 2) and the pressure in the production well at 50 bar.

Fig. 1 shows methane mole fraction at 58% of PVI computed using the MHFE/DG and MHFE/FV methods on a  $40 \times 40$  mesh. The computation time (to 100% PVI) is 2 min for both methods. As can be seen from the figure, both methods provide very similar results. We have carried out calculations for Example 1 and the next three examples using the first-order finite-volume method for the transport equations. The numerical dispersion is very significant compared to the DG and higher-order finite-volume method. For the sake of brevity, these results are not shown.

## 6.2. Example 2

The second problem is the displacement of propane by methane in a vertical 2D domain (i.e. with gravity). Methane is injected in the lower left corner, displacing propane that is produced in the upper right corner. The data of the problem are given in Table 2. The initial pressure is fixed in the production well. The pressure and temperature are chosen so that the mixture stays in single-phase gas state during the whole simulation. The computation time to 100% of PVI on a  $40 \times 40$  grid is 8 min for both methods. Fig. 2 shows methane mole fraction at 20% of PVI computed using the MHFE/DG and MHFE/FV methods. Note the non-symmetry due to gravity effect. Again, both methods provide similar results.

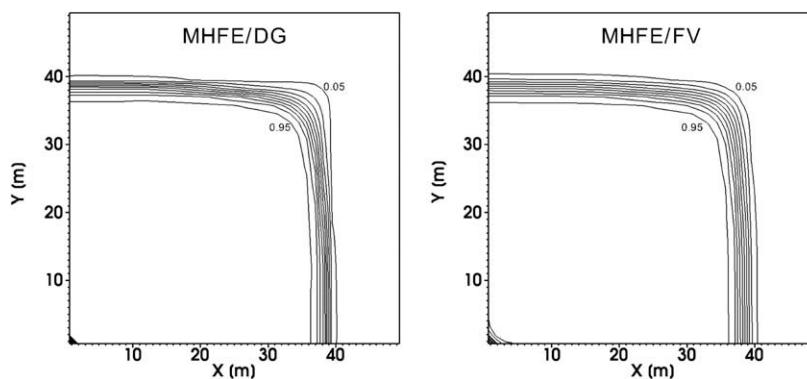


Fig. 1. Methane mole fraction at PVI = 58% (0.69 years) computed on a  $40 \times 40$  mesh by the MHFE/DG method (left) and the MHFE/FV method (right): Example 1.

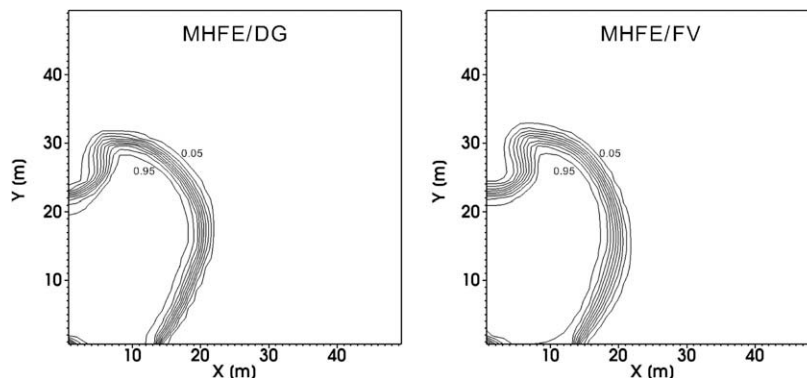


Fig. 2. Methane mole fraction at PVI = 20% (0.24 years) computed by the MHFE/DG (left) and the MHFE/FV (right) methods on a  $40 \times 40$  mesh: Example 2.

Table 3

Relevant data for Examples 3 and 4.

Injection fluid composition (mole fraction)	1.0 $C_1$	0.0 $C_3$
Initial fluid composition (mole fraction)	0.0 $C_1$	1.0 $C_3$
Initial pressure at the bottom (bar)	69	
Temperature (K)	311	
Porosity (fraction)	0.2	
Permeability (md)	10	
Injection rate ( $m^2/day$ ) at $p = 1$ atm, $T = 293$ K	42.5	

6.3. Example 3

The third problem is the displacement of propane by methane in a horizontal 2D domain (i.e. without gravity). Methane is injected in the lower left corner, displacing propane that is produced in the upper right corner. The relevant data are shown in Table 3. Unlike Example 1, the pressure and the temperature are chosen so that a two-phase region develops. In this example, methane, similar to Examples 1 and 2, is a gas but propane, unlike Examples 1 and 2, is in liquid state.

Fig. 3 shows the overall methane mole fraction at 50% of PVI computed using the MHFE/DG and MHFE/FV methods on a  $40 \times 40$  mesh. The computation time was 2 min for MHFE/DG and 3 min for MHFE/FV methods. Both methods provide results that match almost perfectly.

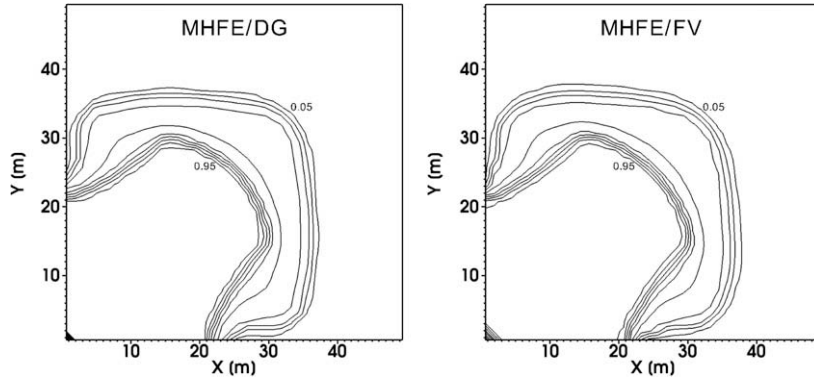


Fig. 3. Overall methane mole fraction at PVI = 50% (1.15 years) computed on a  $40 \times 40$  mesh by the MHFE/DG method (left) and the MHFE/FV method (right): Example 3.

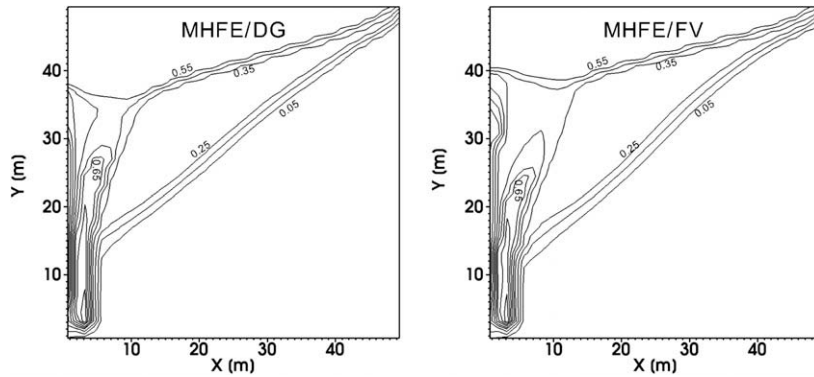


Fig. 4. Overall methane mole fraction at PVI = 50% (1.15 years) computed on a  $40 \times 40$  mesh by the MHFE/DG method (left) and the MHFE/FV method (right): Example 4.

Table 4

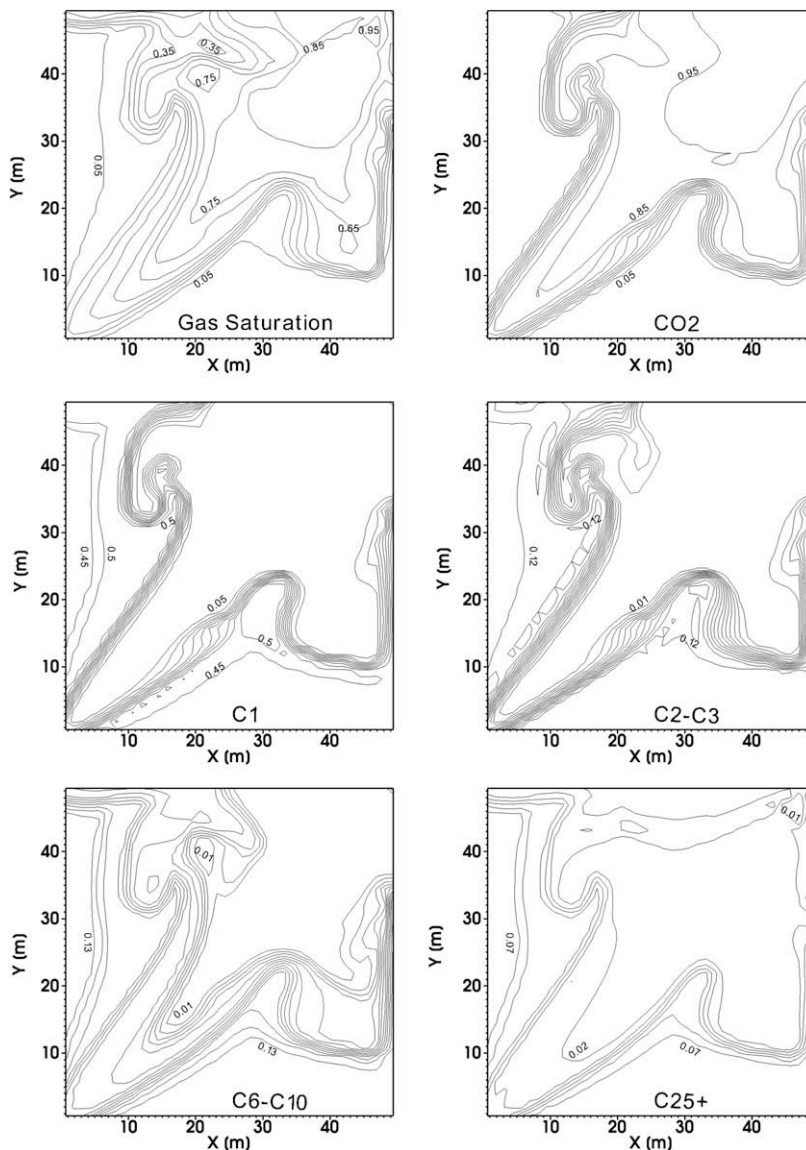
Relevant data for Examples 5 and 6.

Injection gas composition (mole fraction)	1.0 CO <sub>2</sub>	0.0 N <sub>2</sub>
	0.0 C <sub>1</sub>	0.0 C <sub>2</sub> –C <sub>3</sub>
	0.0 C <sub>4</sub> –C <sub>5</sub>	0.0 C <sub>6</sub> –C <sub>10</sub>
	0.0 C <sub>11</sub> –C <sub>24</sub>	0.0 C <sub>25+</sub>
Initial fluid composition (mole fraction)	0.0086 CO <sub>2</sub>	0.0028 N <sub>2</sub>
	0.4451 C <sub>1</sub>	0.1207 C <sub>2</sub> –C <sub>3</sub>
	0.0505 C <sub>4</sub> –C <sub>5</sub>	0.1328 C <sub>6</sub> –C <sub>10</sub>
	0.1660 C <sub>11</sub> –C <sub>24</sub>	0.0735 C <sub>25+</sub>
Initial pressure at the bottom (bar)	276	
Temperature (K)	403.15	
Porosity (fraction)	0.2	
Permeability (md)	10	
Injection rate (m <sup>2</sup> /day) at $p = 1$ atm, $T = 293$ K	133.33	

**Table 5**

Properties of the eight-component mixture in Examples 5 and 6.

Property	CO <sub>2</sub>	N <sub>2</sub>	C <sub>1</sub>	C <sub>2</sub> –C <sub>3</sub>	C <sub>4</sub> –C <sub>5</sub>	C <sub>6</sub> –C <sub>10</sub>	C <sub>11</sub> –C <sub>24</sub>	C <sub>25+</sub>
Accentric factor	0.23900	0.03900	0.01100	0.11783	0.21032	0.41752	0.66317	1.72763
Critical temperature (K)	304.14	126.21	190.56	327.81	435.62	574.42	708.95	891.47
Critical pressure (bar)	73.75	33.90	45.99	46.54	36.09	25.04	15.02	7.60
Molar weight (g/mol)	44	28	16	34.96	62.98	110.21	211.91	462.79
Critical volume (m <sup>3</sup> /kg)	0.00214	0.00321	0.00615	0.00474	0.437	0.00425	0.00443	0.00417
Volume shift parameter	0.0600	–0.2885	–0.0154	–0.0949	–0.0598	0.0466	0.1494	0.4950
<i>Binary interaction coefficients</i>								
CO <sub>2</sub>	0							
N <sub>2</sub>	0	0						
C <sub>1</sub>	0.15	0.1	0					
C <sub>2</sub> –C <sub>3</sub>	0.15	0.1	0.0346	0				
C <sub>4</sub> –C <sub>5</sub>	0.15	0.1	0.0392	0	0			
C <sub>5</sub> –C <sub>10</sub>	0.15	0.1	0.0469	0	0	0		
C <sub>11</sub> –C <sub>24</sub>	0.15	0.1	0.0635	0	0	0	0	
C <sub>25+</sub>	0.08	0.1	0.1052	0	0	0	0	0

**Fig. 5.** Results at PVI = 50% (1.37 years) computed on a 40 × 40 mesh by the MHFE/DG method showing gas saturation, and overall mole fractions of CO<sub>2</sub>, C<sub>1</sub>, C<sub>2</sub>–C<sub>3</sub>, C<sub>6</sub>–C<sub>10</sub>, and C<sub>25+</sub> pseudocomponent: Example 5.

6.4. Example 4

The fourth example, the displacement of propane by methane is studied in a vertical 2D domain (i.e. with gravity). Methane is injected in the lower left corner, displacing propane that is produced in the upper right corner. The data of the problem are given in Table 3. The pressure in the production well is fixed at the initial pressure. Unlike in Example 2, the pressure and the temperature are chosen so that a two-phase region develops. Fig. 4 shows the methane overall mole fraction at 50% of PVI computed on a  $40 \times 40$  grid. The match between the two methods is again very good. The computation time for both methods to 100% of PVI is approximately 45 min for MHFE/DG and 47 min for MHFE/FV.

6.5. Example 5

In this example, we simulate the injection of  $\text{CO}_2$  in a domain saturated with an 8-component hydrocarbon mixture. The initial fluid mixture is in liquid state. The domain is a vertical cross-section of size  $50 \times 50$  m. The components, the composition of the initial and the injected fluid, and other parameters are specified in Tables 4 and 5.  $\text{CO}_2$  is injected in the upper

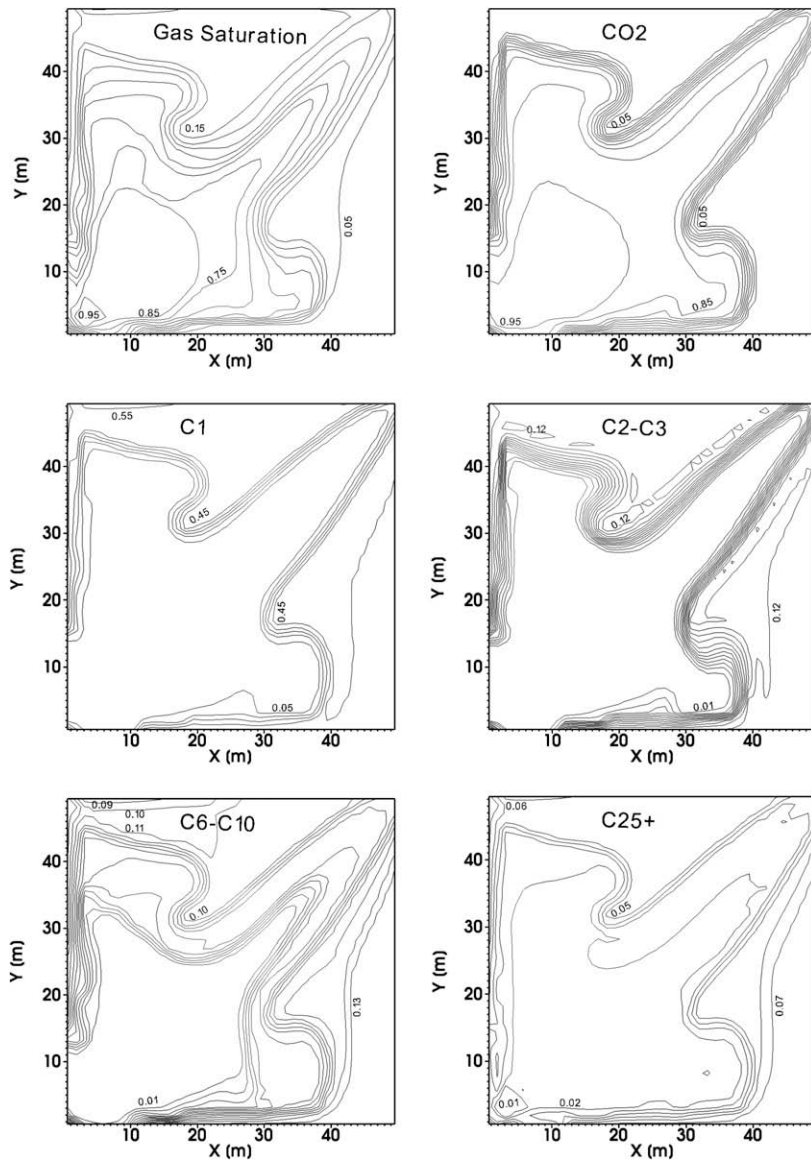


Fig. 6. Results at PVI = 50% (1.37 years) computed on a  $40 \times 40$  mesh by the MFE/DG method showing gas saturation, overall mole fractions of  $\text{CO}_2$ ,  $\text{C}_1$ ,  $\text{C}_2\text{-C}_3$ ,  $\text{C}_6\text{-C}_{10}$ , and  $\text{C}_{25+}$  pseudocomponents: Example 6.

right corner, displacing the hydrocarbon mixture towards the lower left corner. The pressure is fixed in the production well at 276 bar. Under these conditions a two-phase region develops.

Fig. 5 shows gas saturation and overall molar fractions of selected components at 50% of PVI. It is only with the formulation in this paper that the run can be performed. Without our modification the code would break down before achievement of 100% of PVI. The computation time of the MHFE/DG method to 100% of PVI is 60 min on a  $40 \times 40$  grid.

### 6.6. Example 6

In the last example, we simulate the injection of  $\text{CO}_2$  in the bottom of the vertical domain. The components, the composition of the initial and the injected fluid, and other physical parameters are the same as in the previous example (see Tables 4 and 5). The only difference is that this time the injection and production wells are interchanged, i.e. the injection well is located at the bottom of the domain in the lower left corner, and the production is at the top in the upper right corner. The pressure in the production well is fixed at the initial pressure.

Fig. 6 shows the gas saturation and overall molar fractions of selected components at 50% of PVI. The computational time of MHFE/DG method to 100% of PVI is 2 h and 32 min on a  $40 \times 40$  grid.

## 7. Discussion and concluding remarks

In this work, as a result of use of individual component balance equations, we have suppressed spurious oscillations in composition that were leading to crash of the code in the previous works [3,4]. While our suggestion for the use of Eq. (1) rather than Eq. (2) is deceptively simple, the effect on the robustness of the code is significant. This suggestion affects only the higher-order methods, such as discontinuous Galerkin or MUSCL-type finite-volume methods, which require stabilization using a slope limiter.

The use of boundary conditions for total molar flux and total individual component fluxes are also straightforward and result in substantial improved efficiency of the code. Our suggestion in the boundary condition makes the problem formulation consistent. Proper treatment of boundary conditions allows to increase time steps and leads to significant speed up of the code in both MHFE/FV and MHFE/DG methods.

The approximation of phase fluxes described in our work is a key in MHFE method. Without our implementation we have seen code crash.

All aspects of our suggestions relate to two-phase flows, where without them, the use of higher-order methods will not be widespread in some applications such as  $\text{CO}_2$  injection in the subsurface.

In order to show robustness and efficiency of the proposed algorithm, we present six examples of various degree of complexity. The comparison of MHFE/DG and MHFE/FV shows that both methods provide similar results. Generally, FV scheme of MUSCL-type is considered to be cheaper than DG because of lower number of degrees of freedom per element in the case of FV method, but our experiments show that the CPU time difference between the two methods is practically negligible. The two methods are very similar; they only differ in the evaluation of the gradients of the concentrations at the elements. While the DG method provides an evolution equation for the gradients, in higher-order finite-volume methods, the gradient is reconstructed from the neighboring cells. In case of the orthogonal grid, this reconstruction is particularly simple, but this may not be the case when more general unstructured grids are used (see e.g. [20]). The FV method is expected to be faster because it does not include the evaluation of the integral over the element (the second term on the left hand side of (32)) as in DG. However, this step has very little effect on the overall efficiency of the code. The explicit solution of the transport equation requires about 5% of the CPU time while the flash and linear solver take 80–85% and 5–10% of the CPU, respectively. These data correspond to Examples 1–4. In some cases we observed that the computation time of DG was even lower than for FV (see Examples 2 and 3). We have used the MHFE/FV to compute results for Example 6 (results not presented for the sake of brevity). The computation time is 2 h and 28 min which is less than 2 h and 32 min for MHFE/DG. We have presented results of two simulations of  $\text{CO}_2$  injection in a multicomponent hydrocarbon mixture; these are new results that could not be obtained using previous work in the literature in which inappropriate upwinding of mobility coefficients created numerical problems leading to breakdown of the computation at the very beginning.

### Acknowledgments

This work was supported by the member companies of the Reservoir Engineering Research Institute (RERI), Qatar Foundation, and by the project Mathematical Modelling of Multi-Phase Porous Media Flow, number 201/08/P567 of the Czech Science Foundation.

### Appendix A. Raviart–Thomas basis functions and details of the MHFE discretization

We use the lowest order Raviart–Thomas elements [16,17] for which the functions  $\mathbf{w}_{K,E}$  are associated with the rectangle edges of each element  $K$ . These functions defined on a reference element  $K = (0, l_x) \times (0, l_y)$  read as

$$\begin{aligned} \mathbf{w}_{K,B}(x,y) &= \left(0, \frac{y-l_y}{|K|}\right), & \mathbf{w}_{K,T}(x,y) &= \left(0, \frac{y}{|K|}\right), \\ \mathbf{w}_{K,L}(x,y) &= \left(\frac{x-l_x}{|K|}, 0\right), & \mathbf{w}_{K,R}(x,y) &= \left(\frac{x}{|K|}, 0\right), \end{aligned} \tag{41}$$

where the  $B$ ,  $T$ ,  $L$ , and  $R$  denote the bottom, top, left, and right edge in the element  $K$ , respectively. These function are linearly independent and satisfy the following properties

$$\nabla \cdot \mathbf{w}_{K,E} = \frac{1}{|K|}, \quad \mathbf{w} \cdot \mathbf{n}_{K,E'} = \frac{1}{|E|} \delta_{E,E'}, \tag{42}$$

where  $|K|$  denotes the surface area of the element  $K$  and  $|E|$  stands for the length of the edge  $E$ .

Assume that the total molar flux  $\mathbf{q}$  and the vector  $\mathbf{K}\mathbf{g}$  can be represented on the element  $K$  as

$$\mathbf{q}(\mathbf{x}, t)|_K = \sum_{E' \in \partial K} q_{K,E'} \mathbf{w}_{K,E'}(\mathbf{x}), \quad \mathbf{K}\mathbf{g}|_K = \sum_{E' \in \partial K} q_{K,E'}^{Kg} \mathbf{w}_{K,E'}(\mathbf{x}), \tag{43}$$

where  $q_{K,E'} = \int_E \mathbf{q} \cdot \mathbf{n}_{K,E'}$  and  $q_{K,E'}^{Kg} = \int_E \mathbf{K}\mathbf{g} \cdot \mathbf{n}_{K,E} = \mathbf{K}\mathbf{g} \cdot \mathbf{n}_{K,E}|E|$ . Multiplying (14) by  $\mathbf{w}_{K,E}$ , integrating the result over the element  $K$ , and using the Gauss theorem, one obtains

$$\int_K \frac{\mathbf{w}_{K,E} \cdot \mathbf{K}^{-1} \mathbf{q}}{\sum_{\alpha'} c_{\alpha'} \lambda_{\alpha'}} = - \int_K \mathbf{w}_{K,E} \cdot \nabla p + \int_K \rho \mathbf{w}_{K,E} \cdot \mathbf{g} = \int_K p \nabla \cdot \mathbf{w}_{K,E} - \int_{\partial K} p \mathbf{w}_{K,E} \cdot \mathbf{n}_{K,E} + \int_K \rho \mathbf{w}_{K,E} \cdot \mathbf{K}^{-1} \mathbf{K}\mathbf{g}. \tag{44}$$

The right side can be further simplified using the properties of basis functions (42) into

$$\int_K \frac{\mathbf{w}_{K,E} \cdot \mathbf{K}^{-1} \mathbf{q}}{\sum_{\alpha'} c_{\alpha'} \lambda_{\alpha'}} = \frac{1}{|K|} \int_K p - \frac{1}{|E|} \int_E p + \int_K \rho \mathbf{w}_{K,E} \cdot \mathbf{K}^{-1} \mathbf{K}\mathbf{g}. \tag{45}$$

Let  $p_K$  and  $tp_{K,E}$  denote the cell and edge average pressure, respectively. Assuming that the mobilities and densities are constant over the element  $K$ , and using (43), (45) is approximated by

$$\sum_{E' \in \partial K} \frac{q_{K,E'}}{\sum_{\alpha'} c_{\alpha',K} \lambda_{\alpha',K}} \mathbf{A}_{K,E,E'} = p_K - tp_{K,E} + \sum_{E' \in \partial K} \rho_K q_{K,E'}^{Kg} \mathbf{A}_{K,E,E'}, \tag{46}$$

where

$$\mathbf{A}_{K,E,E'} = \int_K \mathbf{w}_{K,E} \cdot \mathbf{K}^{-1} \mathbf{w}_{K,E'}. \tag{47}$$

By inverting the matrix  $\mathbf{A}_K = [\mathbf{A}_{K,E,E'}]_{E,E' \in \partial K}$ , the flux  $q_{K,E}$  can be expressed as

$$q_{K,E} = a_{K,E} p_K - \sum_{E' \in \partial K} b_{K,E,E'} tp_{K,E'} + d_{K,E}, \tag{48}$$

where

$$a_{K,E} = \sum_{\alpha'} c_{\alpha',K} \lambda_{\alpha',K} \sum_{E' \in \partial K} \mathbf{A}_{K,E,E'}^{-1}, \tag{49}$$

$$b_{K,E,E'} = \sum_{\alpha'} c_{\alpha',K} \lambda_{\alpha',K} \mathbf{A}_{K,E,E'}^{-1}, \tag{50}$$

$$d_{K,E} = \mathbf{K}\mathbf{g} \cdot \mathbf{n}_{K,E}|E| \sum_{\alpha'} c_{\alpha',K} \lambda_{\alpha',K} \rho_{\alpha,K}. \tag{51}$$

Note that in our implementation,  $\mathbf{K}$  is assumed to be a scalar constant over the element. If the integral on the right side is computed exactly, we have to invert the  $4 \times 4$ -matrix which is block-diagonal with full  $2 \times 2$  diagonal blocks that reads as

$$\mathbf{A}_K = \left[ \frac{1}{|K|} \int_K \mathbf{w}_{K,E} \cdot \mathbf{w}_{K,E'} \right]_{E,E'} = \frac{1}{6K} \begin{pmatrix} 2 \frac{l_y}{l_x} & -\frac{l_x}{l_y} & 0 & 0 \\ -\frac{l_x}{l_y} & 2 \frac{l_x}{l_y} & 0 & 0 \\ 0 & 0 & 2 \frac{l_y}{l_x} & -\frac{l_y}{l_x} \\ 0 & 0 & -\frac{l_y}{l_x} & 2 \frac{l_y}{l_x} \end{pmatrix}, \tag{52}$$

where  $l_x$  and  $l_y$  are the lengths of the rectangle sides parallel to  $x$  and  $y$  axis, respectively. This matrix is non-singular and can be inverted as

$$\mathbf{A}_K^{-1} = \mathbf{K} \begin{pmatrix} 4 \frac{l_y}{l_x} & 2 \frac{l_y}{l_x} & 0 & 0 \\ 2 \frac{l_y}{l_x} & 4 \frac{l_y}{l_x} & 0 & 0 \\ 0 & 0 & 4 \frac{l_x}{l_y} & 2 \frac{l_x}{l_y} \\ 0 & 0 & 2 \frac{l_x}{l_y} & 4 \frac{l_x}{l_y} \end{pmatrix}. \tag{53}$$

The rows and columns of both matrices correspond to the edges of the elements in the rank right, left, top and bottom. It is known that the resulting matrix of the MHFE method is not the  $M$ -matrix which can lead to oscillations in the solution (see [18]). Chavent and Roberts [19] have recommended to evaluate the integral in (52) using the following low-order quadrature rule

$$\int_K \varphi(x) dx \approx \frac{|K|}{4} \sum_{j=1}^4 \varphi(x_j), \quad (54)$$

where  $x_i$  denotes coordinates of the element vertices. With this mass-lumping technique, the matrix  $\mathbf{A}_K$  is approximated by

$$\mathbf{A}_K = \left[ \frac{1}{|\mathbf{K}|} \int_K \mathbf{w}_{K,E} \cdot \mathbf{w}_{K,E'} \right]_{E,E'} \approx \frac{1}{2\mathbf{K}} \begin{pmatrix} \frac{l_x}{l_y} & 0 & 0 & 0 \\ 0 & \frac{l_x}{l_y} & 0 & 0 \\ 0 & 0 & \frac{l_y}{l_x} & 0 \\ 0 & 0 & 0 & \frac{l_y}{l_x} \end{pmatrix} \quad (55)$$

whose inversion is

$$\mathbf{A}_K^{-1} \approx \mathbf{K} \begin{pmatrix} 2\frac{l_y}{l_x} & 0 & 0 & 0 \\ 0 & 2\frac{l_y}{l_x} & 0 & 0 \\ 0 & 0 & 2\frac{l_x}{l_y} & 0 \\ 0 & 0 & 0 & 2\frac{l_x}{l_y} \end{pmatrix}. \quad (56)$$

## Appendix B. Basis functions and details of the discontinuous Galerkin FEM discretization

The basis functions  $\varphi_{K,l}$  defined on a reference element  $K = (0, l_x) \times (0, l_y)$  read as

$$\varphi_{K,1}(x, y) = 1, \quad \varphi_{K,2}(x, y) = \frac{2}{l_x} \left( x - \frac{l_x}{2} \right), \quad \varphi_{K,3}(x, y) = \frac{2}{l_y} \left( y - \frac{l_y}{2} \right). \quad (57)$$

The weighting factors  $cz_{i,K}^l$  ( $l = 1, 2, 3$ ) can be then interpreted as the average value of molar concentration over the element  $K$ , and differences between the central value and the values at the right and top edges, respectively. The matrix elements appearing in (32) are defined by the following integrals

$$M_{j,l}^K = \int_K \varphi_{K,j} \varphi_{K,l}, \quad M_j^E = \frac{1}{|E|} \int_E \varphi_{K,j},$$

$$M_{j,l}^{K,E} = \int_K \varphi_{K,l} \mathbf{w}_{K,E} \cdot \nabla \varphi_{K,j},$$

where we assume that the phase fluxes fields on the element  $K$  can be approximated as

$$\mathbf{q}_{\alpha,K} = \sum_{E \in \partial K} q_{\alpha,K,E} \mathbf{w}_{K,E}$$

using the vector basis functions from the mixed-hybrid finite-elements. The integrals can be readily evaluated to obtain

$$M^K = [M_{j,l}^K] = \begin{pmatrix} 1 & 0 & 0 \\ 0 & \frac{1}{3} & 0 \\ 0 & 0 & \frac{1}{3} \end{pmatrix} |K| \quad (58)$$

for matrix  $M^K$ . The matrices  $M^E$ , where the edges  $E$  are denoted by  $T$ ,  $B$ ,  $L$ , and  $R$  (top, bottom, left, and right, respectively), read as

$$M^T = [M_j^T] = \begin{pmatrix} 1 \\ 0 \\ 1 \end{pmatrix}, \quad M^B = [M_j^B] = \begin{pmatrix} 1 \\ 0 \\ -1 \end{pmatrix}, \quad (59)$$

$$M^R = [M_j^R] = \begin{pmatrix} 1 \\ 1 \\ 0 \end{pmatrix}, \quad M^L = [M_j^L] = \begin{pmatrix} 1 \\ -1 \\ 0 \end{pmatrix}. \quad (60)$$

Using the same notation for the edges, the elements of matrices  $M^{K,E}$  are evaluated as

$$\begin{aligned}
 M^{K,T} &= [M_{j,l}^{K,T}] = \begin{pmatrix} 0 & 0 & 0 \\ 0 & 0 & 0 \\ 1 & 0 & \frac{1}{3} \end{pmatrix}, & M^{K,B} &= [M_{j,l}^{K,B}] = \begin{pmatrix} 0 & 0 & 0 \\ 0 & 0 & 0 \\ -1 & 0 & \frac{1}{3} \end{pmatrix}, \\
 M^{K,R} &= [M_{j,l}^{K,R}] = \begin{pmatrix} 0 & 0 & 0 \\ 1 & \frac{1}{3} & 0 \\ 0 & 0 & 0 \end{pmatrix}, & M^{K,L} &= [M_{j,l}^{K,L}] = \begin{pmatrix} 0 & 0 & 0 \\ -1 & \frac{1}{3} & 0 \\ 0 & 0 & 0 \end{pmatrix}.
 \end{aligned}
 \tag{61}$$

## References

- [1] R.J. Leveque, Finite volume methods for hyperbolic problems, Cambridge Texts in Applied Mathematics, Cambridge University Press, 2002.
- [2] J.E.P. Monteagudo, A. Firoozabadi, Control-volume model for simulation of water injection in fractured media: incorporating matrix heterogeneity and reservoir wettability effects, SPEJ (2007).
- [3] H. Hoteit, A. Firoozabadi, Multicomponent fluid flow by discontinuous Galerkin and mixed methods in unfractured and fractured media, Water Resour. Res. 41 (2005) W11412, doi:10.1029/2005WR004339.
- [4] H. Hoteit, A. Firoozabadi, Compositional modeling by the combined discontinuous Galerkin and mixed methods, SPEJ (2006).
- [5] Z. Chen, B. Cockburn, J.W. Jerome, C.-W. Shu, Mixed-RKDG finite element methods for the 2D hydrodynamic model for semiconductor device simulation, VLSI Des. 3 (2) (1995) 145–158.
- [6] G. Ács, S. Doleschall, É. Farkas, General purpose compositional model, SPEJ 25 (4) (1985) 543–553 (SPE-10515-PA).
- [7] J. Lohrenz, B. Bary, R. Clark, Calculating viscosities of reservoir fluids from their compositions, J. Pet. Technol. 16 (1964) 1171–1176.
- [8] A. Firoozabadi, Thermodynamics of Hydrocarbon Reservoirs, McGraw-Hill, New York, 1999.
- [9] D.-Y. Peng, D.B. Robinson, A new two-constant equation of state, Ind. Eng. Chem. Fundam. 15 (1) (1976) 59–64.
- [10] B. van Leer, Towards the ultimate conservative difference scheme. I. The quest of monotonicity, Springer Lect. Note Phys. 18 (1973) 163–168.
- [11] B. van Leer, Towards the ultimate conservative difference scheme. II. Monotonicity and conservation combined in a second order scheme, J. Comput. Phys. 14 (1974) 361–370.
- [12] B. van Leer, Towards the ultimate conservative difference scheme. III. Upstream-centered finite-difference schemes for ideal compressible flow, J. Comput. Phys. 23 (1977) 263–275.
- [13] B. van Leer, Towards the ultimate conservative difference scheme. IV. A new approach to numerical convection, J. Comput. Phys. 23 (1977) 276–299.
- [14] B. van Leer, Towards the ultimate conservative difference scheme. V. A second order sequel to Godunov's method, J. Comput. Phys. 32 (1979) 101–136.
- [15] P.H. Sammon, An analysis of upstream differencing, SPE Reserv. Eng. (1988) 1053–1056.
- [16] F. Brezzi, M. Fortin, Mixed and Hybrid Finite Element Methods, Springer, New York, 1991.
- [17] P. Raviart, J. Thomas, A mixed hybrid finite element method for the second order elliptic problem, Lect. Note Math. Ser., vol. 606, Springer, New York, 1977.
- [18] A. Younes, P. Ackerer, F. Lehmann, A new mass lumping scheme for the mixed hybrid finite element method, Int. J. Numer. Method Eng. 67 (2006) 89–107.
- [19] G. Chavent, J.E. Roberts, A unified physical presentation of mixed, mixed-hybrid finite elements and standard finite difference approximations for the determination of velocities in waterflow problems, Adv. Water Resour. 14 (6) (1991) 329–348.
- [20] M. Feistauer, J. Felcman, Straškraba, Mathematical and Computational Methods for Compressible Flow, Clarendon Press, Oxford, 2003.